Assessment of homogeneity of the shear-strain pattern in Al-7wt%Si casting alloy processed by high-pressure torsion

C.M. Cepeda-Jiménez[a], A. Orozco-Caballero[a], J.M. García-Infanta[a], A.P. Zhilyaev[b], O.A. Ruano[a], F. Carreño[a]

[a]*Department of Physical Metallurgy, CENIM, CSIC, Av. Gregorio del Amo 8, 28040 Madrid, Spain*

[b]*Institute for Metals Superplasticity Problems, Russian Academy of Science, 39 Khalturina, 450001 Ufa, Russia*

Abstract

An as-cast Al-7 wt% Si alloy was subjected to processing by high-pressure torsion (HPT) at room temperature, through ¼, ½, 1 and 5 turns at a pressure of 6 GPa and two rotation speeds, 0.1 and 1 rpm. Vickers microhardness was measured along diameters of HPT disk surfaces. The final hardness values were higher than in the initial as-cast condition and, unexpectedly, nearly constant under all different processing conditions, and along the diameter disks. The microstructure was characterized by optical and scanning electron microscopy. The as-cast microstructure comprises equiaxed primary α dendrite cells embedded in the Al-Si eutectic constituent. The morphology and distribution of the eutectic constituent in the HPT processed materials is used to delineate the shear strain, which was analyzed in the cross-section planes of the disks. A high degree of homogeneity in the imposed shear strain throughout the samples was observed, being congruent with the ideal rigid-body torsion. In addition, the high compressive pressure applied, causing compressive strain prior to the torsional strain, is responsible for the deformation-induced precipitation of small Si particles and for the (sub)grain refinement in the primary Al constituent. The role of torsional strain is that of increasing monothonically the redistribution of the eutectic silicon and the misorientation of the (sub)grains.

Keywords: B. Al-Si alloys; C. High pressure torsion; D. Deformation-induced precipitation; D. Torsional strain pattern; D. Grain refinement.

*Corresponding author (C.M. Cepeda-Jiménez; formerly CENIM-CSIC).

Present address: IMDEA Materials Institute, C/Eric Kandel 2, 28906 Getafe, Madrid, Spain; Tel.:+34 91 549 34 22; fax: +34 91 550 30 47

E-mail address: carmen.cepeda@imdea.org

1. Introduction

Severe plastic deformation (SPD) has been well documented as a resource for producing bulk ultrafine-grained materials [1]. The main characteristic of all SPD methods is the accumulation of large plastic strain without any notable change in the sample dimensions [2]. Among these techniques, high pressure torsion (HPT) is the most effective processing to produce exceptionally small grain sizes [3-5].

The HPT sample is usually in the form of a thin disk and it is processed in an HPT facility where it is subjected to a compressive load and concurrent torsional deformation [4-6]. The applied compressive pressure prevents the occurrence of cracking and, thereby, enables the processing of difficult-to-work alloys, such as aluminium casting alloys [7,8].

It is has been widely reported the strain non-uniformity during HPT processing [8,9]. However, most of the previous investigations based on HPT processing have been performed using pure metals or single-phase solid solution alloys [10-12], or multiphase alloys with only a small amount of second phase [13,14] wherein at large strains the prior grain structure can no longer be distinguished [15]. This makes difficult to clearly visualize the shear strain imposed during HPT, and whether it is or not homogeneous throughout the sample. From the point of view of the use of materials produced by HPT, the homogeneity of the final product is of critical importance [8].

Extensive experimental efforts have been made to explain the deviations of HPT shear strain from the ideal rigid-body situation. In fact, the simple shear strain equation $\gamma=2\pi Nr/h$ (1), where r and h are the radius and height (or thickness) of the disk, respectively, and N is the number of turns, was developed mathematically for a rigid-body situation [16,17].

In a previous report about processing by HPT of a duplex stainless steel [18], in which two phases coexist with approximately the same volume fractions, the HPT-induced shear-strain pattern revealed that shear strain spreads parallel to the radial directions in the very early stages of HPT processing and the formation of local shear vortices and a double-swirl shear-strain pattern at the centre of the HPT discs. After these remarkable shear strain features authors claim that the microstructural evolution during HPT is more complex than the ideal rigid-body situation [18]. However, it is our contention that this deviation of the ideal situation depends on the plasticity of the multiphase system selected to evaluate the HPT imposed strain. Most of recent reports published to date [10,11,17-20] reveal strong deviations from the theoretical relationship of the shear strain imposed by HPT because of the selection of the two-phase or multiphase materials, where the little difference between plasticity of the

phases leads to a strain non-uniformity, complicating the real assessment of the deformation imposed by HPT processing.

On the other hand, as-cast alloys often contain heterogeneous distributions of non-deforming particles [21,22]. Accordingly, in recent works, the eutectic constituent in as-cast Al-7wt%Si alloy provided a non-deforming stable marker that delineated the shape change in the microstructure during repetitive ECAP [21-23]. Thus, in this work the as-cast Al-7wt%Si alloy has been selected to delineate the homogeneity degree of the imposed strain by HPT, and thereby aid in establishing the congruence between the observed and expected shape change after processing.

In addition, most of the studies conducted to date analyze the level of deformation imposed on the sample during HPT on the distributions of hardness values on the disk surfaces [8,18,24-26]. As it will be demonstrated, microhardness distribution is not a good parameter to reach conclusions on the degree of strain homogeneity along the radial directions of the samples. This is because the microhardness, in alloys such as Al-7wt%Si with little precipitation hardening, depends mainly on the final (sub)grain size, which, in absence of recrystallization processes, is best determined by the stress withstood by the sample during processing than by strain [27,28].

Therefore, in the present investigation the evolution of the shear strain patterns, delineated by non-deforming Si particles of the eutectic constituent, has been analyzed. This analysis has been conducted over the cross-sections in an as-cast Al-7wt%Si alloy subjected to HPT at room temperature for different numbers of turns and two strain rates, by measuring the primary dendritic arm spacing variations as a function of radius. In addition, the mechanical behaviour is examined by Vickers microhardness testing and related to the analyzed microstructure.

2. Experimental procedure

Pure Al (99.99 wt%) and an Al–12.3 wt% Si–0.02wt% Na alloy were melted and casted into a mould to produce an ingot having dimensions of 400 mm × 250 mm × 40 mm. Emission spectroscopy of the resulting material revealed a composition (in wt%) of 7.0% Si, 0.3% Fe and balance Al. Disk samples for HPT were machined with dimensions ~1 mm thick and ~10 mm in diameter.

Samples were then subjected to HPT processing at room temperature using a quasi-constrained HPT facility, where lateral flow of the material is partially restricted. The principles of HPT processing are depicted schematically in Fig. 1a and more details are given elsewhere [4]. The imposed pressure was maintained constant during processing at 6.0 GPa, and separate disks were processed through totals of ¼, ½, 1, and 5 turns, at a fixed speed of either 0.1 or 1 rpm, respectively. The final thickness of the HPT samples

was ~0.9 mm. Minor differences in the specimen thicknesses after different conditions of HPT processing were observed.

HPT processed samples were characterized using both optical and scanning electron microscopy on the cross-section planes, and microhardness measurements on the top plane. Accordingly, after processing, the disks were sectioned along their cross-section plane that passed through the centre of the disks, as shown in Fig.1b, and mounted in epoxy resin.

Both top and cross-sectional planes were ground with abrasive paper and polished with diamond paste, and then electropolished in a 30% nitric acid solution in methanol at -28 ºC and 17 V. Microstructure, both in the central regions of the disks and near the edges, was observed by scanning electron microscopy (SEM), using a JEOL JSM 6500F equipment with field emission gun. Grain size was measured on the primary Al constituent for all the processed conditions from SEM images obtained using backscattered electrons. The mean linear intercept method was employed, without discriminating between high- and low-angle boundaries. The dendrite thicknesses on the cross-sectional planes, delineated by the eutectic Si particles, and the eutectic Si particle size were measured by optical microscopy. Both optical and scanning electron micrographs were analyzed using the Sigma Scan Pro software. More than 550 precipitates and 200 grains for each processing condition were analyzed. Particles and grain size data fell into lognormal distributions, so the geometric mean value was chosen as a measure of their size.

Vickers microhardness was measured along diameters of HPT disk surfaces (Fig. 1b) using a Matsuzawa Seiki MHT-1 microhardness tester, with a load of 1kg and a dwelling time for each separate measurement of 15 s for the un-processed samples, and a load of 100 g for 15 s for the HPT processed materials. The distance from each indentation centre to the centre of the disk was measured using the Sigma Scan Pro image analysis software.

3. Results

The microstructure of the as-cast Na-modified Al-7 wt% Si alloy is shown in Fig. 2a. The starting microstructure consists of the primary Al matrix surrounded by the interdendritic network of eutectic constituent. This eutectic phase contains a distribution of mainly irregular Si fibres, and a small volume fraction of needle-like Al_5FeSi phase consequence of Fe impurities on the alloy. The primary Al dendrite cell size was measured from optical micrographs using the mean linear intercept method. These cells appear approximately spherical in shape although their sizes vary throughout the casting due to solidification rate effects [22]. Fig. 2b shows the dendrite

size distribution histogram for the as-received sample determined by measuring about 1000 dendrites in the as-cast Al-7wt%Si alloy. The average dendrite cell size, *l*, is ~54 μm.

Fig. 3a-c shows montages of optical micrographs of the entire top surface deformation microstructure of HPT disks strained through 0.25, 0.5 and 1 turns, respectively, using a rotation speed of 0.1 rpm. In addition, Fig. 3d shows details of each disk surface at higher magnification. It is observed from Fig. 3a that the initial eutectic shape is apparently retained (the primary α cells are similar in size to those in the as-cast material) in the central area of the disk after 0.25 turns, with some distortion of the dendrite shape in the periphery regions. After 0.5 (Fig.3b) and 1 (Fig.3c) turns, the initial dendrite shape is only retained close to the disk centre. Especially after 1 turn (Fig. 3c), the primary and eutectic constituents appear elongated in the shear flow direction, as it is clearly observed in the magnified micrograph. It can be observed from these micrographs that the primary and eutectic constituents, i.e. the dendrite shape, remain distinct even until strains as large as γ~16, as reached on the disk periphery after 0.5 turns.

On the other hand, shear-strain patterns were analyzed on half cross-sections due to its complexity on the top and bottom surfaces of the disks. This is because the dendrites form arcs elongated in the direction of the torsional straining, making difficult any quantitative analysis. Accordingly, Fig. 4a shows, as an example, an overview of the entire half cross-section of the disk processed through 0.25 turns of HPT at room temperature, using a rotation speed of 0.1 rpm. Since HPT processing presents radial symmetry, any half cross-section considered will be representative for any other maximum section across each disk. In addition, Fig. 4b displays three magnified details of different areas marked with red rectangles in Fig. 4a, between the disk centre and the edge. Firstly, from Fig. 4a it is clearly observed that the Al-7wt% Si alloy deformed by HPT has a deformation structure largely comprised, due to the high initial pressure (6 GPa), which fills the gap between the anvils. In addition, it is also apparent that there is a thin extruded ribbon of material around the periphery of the disk due to the outflow of material through the gap between the top and bottom anvils by the quasi-constrained nature of the processing [6]. Furthermore, from the top and bottom edges of the disk it can be seen zones where neither the primary nor the eutectic can be discerned in the images. It is apparent that an additional localized interaction between the anvil rugosity and the sample is produced. These excessively deformed regions have not been considered in our later analysis.

On the other hand, from Fig.4b at higher magnification it is observed that the primary Al dendrite cells appear to be distorted by progressive shearing to the periphery

to elliptical shapes in the cross-section planes. This distortion appears to be monotonic and homogeneous in nature and the eutectic spacing, or dendrite thickness, decreases with increasing strain in the radial direction.

Fig. 5 shows half cross-sections of HPT disks processed through 0.25, 0.5, 1 and 5 turns at a rotation speed of 1 rpm. In order to evaluate the strain homogeneity across the HPT disks under different processing conditions by the eutectic particle redistribution, equidistant vertical lines from the disk centre were drawn until the dendrite morphology could not be observed, which it was possible up to a shear strain $\gamma > 20$.

Fig. 5 provides a clear representation of the primary dendrite evolution with the increase of torsional straining. For N=5, the dendrite cease to be discernable at an small distance to the center of the disc. The primary and eutectic constituents of the as-cast condition are still discernible at low shear strains (N=0.25-0.5) and the increase in shear strain, i.e. increasing the number of turns, leads to a homogeneous and uniform distribution of Si particles where neither the eutectic nor the primary constituent may be discerned. This is clearly observed in the periphery of the HPT disk after 1 turn, and more easily and faster after 5 turns, where the microstructure is practically homogeneous throughout whole disk and the evidence for alignment with the torsional straining has almost disappeared. Accordingly, from these images, average dendrite thickness values in the selected positions were obtained as a function of the disk radius.

Fig. 6 shows the distributions of the average dendrite thickness at the cross-section of the disks, as a function of the distance from the centre of each disk for 0.25, 0.5, 1 and 5 turns and two rotation speeds of 1 (Fig. 6a) and 0.1 rpm (Fig. 6b). As commented, processing by HPT involves the progressive thickness reduction together with progressive elongation of the primary Al dendrite cells, and the level of strain is dependent upon the magnitude of rotation imposed on the sample. Thus, the elliptic shape cells will become thinner and longer as the shear strain increases, i.e. at the highest rotation number and close to the disk periphery, as it is observed from Fig.6. Low levels of strain are imposed for low rotation degree and especially near the disk centre, where the dendrite thickness after 0.25 turns is practically the same than that for the as-received material after the initial compression. However, the thickness measurement in the centre should be taken with care due to the difficulty to be determined since, in spite of the fact that the torsional deformation in the disk centre should be cero, according to equation (1), the high strain levels produced immediately next to the central point, especially after 1 o 5 turns, are reflected in the dendrite shape. Therefore, large deviations in the dendrite thickness measure are obtained just in the centre of the disks.

In Figure 7, the average dendrite thickness for all HPT processed samples is plotted as a function of shear strain, γ, calculated from Eq.1. To calculate the shear strain it is necessary to consider an appropriate value for the thickness of the disk, *h*. In this study, the final thickness of the processed disk has been considered. Nevertheless, it has been reported [29] that in practice the precise value selected for *h* has only a minor effect on the estimated values of γ. It is apparent, from Fig. 7, that the dendrite thickness decreases progressively with increasing strain until reaching saturation. The dendrite thickness values corresponding to the disk centre, where the strain is zero, are anomalous, as previously commented, due to the fact that the dendrite shape in this point reflects the strain of the immediately next regions. On the other hand, the influence of strain rate is small. It is apparent, from the observed trend, that the torsional strain is produced in a homogeneous way. The saturation level coincides with the strain point where dendrite thickness could not be measured anymore, due to the fact that neither the eutectic nor the primary constituent could be discerned. According to Fig. 7 this saturation strain is achieved at about $\gamma > 20$, and as will be discussed below, it is related to the volume fraction and size of the silicon particles after processing.

Figure 8 shows the hardness distribution values along two disk diameters for each processing condition. Different numbers of turns from 0.25 to 5, and two rotation speeds of 1 (Fig. 8a) and 0.1 rpm (Fig. 8b) have been considered. The lower broken line included in both graphics shows an average hardness value of ~44 HV for the as-cast and unprocessed Al-7wt%Si alloy. It is clear from the measurements that the hardness values increase significantly to average values ranged between ~65 HV for the samples processed through 0.25-1 turns, and ~70 HV after conducting 5 turns. In general, these values are maintained reasonably constant across the disk diameter and they do not show clear trends neither with the turn number nor with the rotation speed. Likewise, a small dependence of the strain rate during HPT processing on hardness values and average grain size has been previously reported [30]. In addition, in contrast to other results [4,5,10,31-42], there are no lower hardness values in the centre of the disks, or even the increase in the number of turns from 0.25 to 5 does not produce a noticeable improvement in the HV values.

Thus, it is apparent from the measurements depicted in Fig.8 that there must have been a significant microstructural change with respect to the as-cast microstructure, and from the early stage of HPT processing, because high microhardness increase is already observed after only 0.25 turns, even near the disk centre where little torsional strain is expected. This apparent controversy with other reported results will be discussed in the following.

4. Discussion

In the present study, severe plastic deformation was imposed on a hypoeutectic Al–7 wt.% Si alloy using HPT processing, through ¼, ½, 1 and 5 turns at a pressure of 6 GPa and two rotation speeds, 0.1 and 1 rpm. After the initial compression and HPT shearing, the aluminium dendrites and eutectic constituents become elongated in the torsional flow direction. At the same time, the thickness of the dendrites decreases in the cross-section so that the volume is preserved. Thus, quantitative microstructural analysis of the evolution of the primary and eutectic constituent morphologies in this alloy can be performed.

On the other hand, from the results shown previously, it is apparent that the microharness values are generally uniform across the diameters of the disks. Even after small torsional strains with low number of turns, a lower hardness in the centre of the disks, respect to the periphery, is not observed. These findings do not agree with previous studies where in general, as reported in most metals, the hardness increases with increasing strain and then reaches a constant or equilibrium value [43]. The strengthening achieved by HPT processing of this Al-7 wt% Si alloy will be analyzed in terms of grain refinement and deformation-induced precipitation due to the high initial compressive pressure and the strain that this pressure produces.

4.1. Assessment of the "macrodeformation" homogeneity

The following discussion tries to demonstrate that the selection of the dual-phase Al-7wt%Si alloy, consisting of non-deforming Si particles embedded in a deformable aluminium matrix, allows analyzing whether the eutectic constituent exhibits shape changes that could be congruent with the ideal rigid-body torsion. Other dual-phase materials [18,29] selected to follow the torsional strain lead to ambiguous conclusions due to the similar plasticity of the constituent phases, observing mixture of phases and local strain hardening effects between phases during processing. Accordingly, it can be expected that the more similar the plasticity between phases, the higher the distortion of the shear strain patterns and heterogeneity of the HPT processing.

Our observations of the dendrite morphologies on cross-section planes show a gradual strain evolution with increasing numbers of turns, as observed for 0.25 turns in Fig.4. Accordingly, the dendritic cells deform and rotate with respect to the torsion axis to form elongated ellipses, leading to monotonic shear-strain patterns with a symmetric distribution of elliptic dendrites across the disk radius, as showed in Fig. 5.

At each location along the lines drawn in Fig. 5, thickness of deformed primary α cells were measured and averaged and the local strain was calculated from the relationship included in equation (1). The results of this procedure are depicted in a

logarithmic plot in Fig. 9 as the average thickness of the dendritic cells in the Al-7wt%Si alloy as a function of the theoretical shear strain throughout the HPT disk. These data indicate that a power-law inverse relationship exists between dendrite thickness and the imposed shear strain by HPT processing. Furthermore, as preliminary studies [6] showed, the strain rate has only a minor effect on the shear strain patterns. This can be observed in Fig. 9, where measurements carried out at two different strain rates perfectly fit in the same curve. Thus, this nearly linear relationship between dendritic thickness, marked by the rigid eutectic particles, and the theoretical shear strain allows assuming that the torsional strain is homogeneous throughout the disk radius, even until the primary α dendrites cannot be discerned anymore (γ>20).

As commented previously, the strain necessary to obtain particle homogenization is a function of the volume fraction and size of the silicon particles after processing. Accordingly, the average three-dimensional distance between the particles (λ) of a phase embedded into a matrix for a random and homogeneous distribution can be defined as [44]:

$$\lambda = \frac{1}{2} d \left(\sqrt{\frac{2\pi}{3 f_v}} - \sqrt{\frac{8}{3}} \right) \quad (2)$$

where the parameter λ takes into account characteristics of the particles such as volume fraction (f_v) and average particle size (d).

Fig. 10 illustrates optical micrographs (Fig.10a) and the particle size distribution histogram (Fig. 10b) of Al–7 wt% Si samples after HPT processing by 5 turns and 1 rpm. After processing, the initial rod-shaped particles present in the as-cast sample are no longer present, and they have been replaced by more equiaxed particles due to the high compression pressure and strain. It has been reported [45,46] that large and elongate particles are very prone to cracking during severe plastic deformation due to the fact that the load transfer process for this morphology is very efficient. Thus, it is our contention that the Si and Al_5FeSi particles were broken during the initial compression pressure, and the later torsional strain is not determinant in the final particle size due to the fact that the high hydrostatic pressure during HPT processing, together with redistribution of Si particles on the soft Al matrix, favour the stress redistribution on the sample, reducing the potential for additional crack nucleation and particle fracture.

Therefore, taking into account that the volume fraction of undeformable Si particles in the Al-7wt%Si alloy is approximately 0.07 [47], and according to the particle size histogram (Fig.10b), the average silicon particle size is about 2.5 μm, the average distance between particles (λ) for an homogenous particle distribution calculated from

equation (2) is ~4.8 μm. It is worth noting that this distance coincides with the saturation thickness in Fig.7 where neither the eutectic and the primary constituent may be discerned. Therefore, a uniform distribution of particles in the aluminium matrix is obtained after a critical strain, which cannot be modified with additional torsional straining. This limit strain, γ~20 , which is achieved after ~0.5 turns at the disk periphery, would be enough to assure particle homogenization and improvement of mechanical properties of the Al-7wt%Si alloy. As seen in Fig. 8, although the microhardness is similar after different HPT processing conditions, high degree of particle homogenization is necessary to achieve good combination of strength and ductility, as it was reported previously [22]. In this previous work, it was demonstrated that the geometrical redistribution of the eutectic constituent achieved by ECAP routes A and B_A increases ductility because it forces the crack through the primary Al matrix, where its propagation is more difficult than through the initial brittle eutectic constituent. Thus, this eutectic homogenization may facilitate forming processes, as well as improve service performance of cast metal components.

As a conclusion of this section, the non-deformability of the eutectic particles, acting like rigid bodies, allows depicting the true imposed torsional strain until particle homogenization is achieved. According to our results, in this two-phase system, shear strain patterns are not affected by the microstructure changes occurred in the aluminium matrix, such as strain hardening, grain refining etc. Therefore, it can be said that HPT processing does not intrinsically causes heterogeneity, as it has been frequently asserted [9,20].

4.2. Grain refining and Vickers microhardness

In most metals [5,10,31-42] the microhardness values in the central region are lower than at the edge of the processed disks in the beginning of straining, but after some number of turns saturation of microhardness is reached throughout the sample. Furthermore, some of these studies [24-26] claim that the microhardness measured in individual HPT samples can be well related to the shear strain. However, in the present study, a relatively uniform hardness distribution along the disk diameter has been obtained (Fig.8), and a clear dependence of hardness with strain (total number of turns) or rotation speed is not observed. Thus, the immediate microhardness increase observed after small number of turns (scarce torsional strain), and its nearly constant value across the disk diameter (Fig. 8) must be attributed to other variables different from torsional strain. These variables must be related to the applied initial pressure and compressive strain, and its influence on microstructure through grain refinement, strain hardening and precipitation from solid solution in the as-cast alloy. As it has been observed in Fig.

4 and 5 the initial applied compressive pressure, P, produces a compressive strain and thus, an important distortion of the dendrites before torsional straining, as observed in the disk centre processed by 0.25 turns. Previous results on an Al-6061 aluminium alloy [36] showed that the initial applied pressure is an important variable, leading to a significant increase in hardness across the disks even without any torsional straining. In our study, the homogeneity in microhardness can be explained by the resulting microstructure after the high initial pressure.

Fig. 11 shows backscattered electron micrographs at two magnifications of the matrix grain microstructure for the HPT processed Al-7wt%Si samples through 0.25 turns (Fig.11a and b) on the disk center, and after 5 turns (Fig.11c and d) on the disk periphery. Both samples were HPT processed under 6 GPa and 1 rpm.

At the periphery of processed disks by 5 turns (with high imposed torsional strain, Fig.11c and d) very fine, equiaxed, well-defined and easily measurable grains with less than 200 nm are obtained, as expected. However, after only 0.25 turns and near the disk centre (Fig.11a and b), where very low levels of torsional strain have been imposed, very fine grain sizes, ~200 nm in size, can be also clearly observed. Thus, a substructure in form of dislocation networks and cells appears during the high initial compressive pressure, as a result of the applied compressive stress and the resulting compressive strain. It has been reported that the dislocation density in materials processed by HPT depends on the applied hydrostatic pressures [48], and thus, the more dislocations are produced and stored, the more grain boundaries can be built from them. This initial dislocation network after the high initial compressive pressure, without additional torsional strain, is constituted by low angle dislocation boundaries, showing a diffuse appearance and small misorientation (Fig.11a and b). The increase in strain during HPT processing by increasing the number of turns leads to a gradual increase in their misorientation up to their final transformation into high angle boundaries at large strain [49], as observed in Fig.11c and d after 5 turns, with clear grain contrast.

Additionally, in Fig.11b and d, it is observed the presence of small Si particles (<100nm in size) within the aluminium matrix, both after 0.25 and 5 turns. Previous EDX measurements [50,51] revealed that following solidification of the as-cast alloy, 1.6wt% Si is retained in supersaturated solid solution within the primary Al dendritic cells. Moreover, before HPT processing, inspection of the primary Al dendrite cells for the as-received samples, using both SE and BSE modes in the FEG–SEM, was also performed and these small precipitates were not detected in the Al matrix. Thus, the absence of these small precipitates in the as-received unprocessed samples corroborates that precipitation is induced by deformation. This deformation-induced precipitation of fine Si precipitates in Al-7wt% Si alloy from the supersaturated solid solution has been

previously reported under different thermo-mechanical processing conditions [52]. Recent studies demonstrated that the samples with the lowest initial Si solid solution concentration led to a larger grain size than that for the more supersaturated ones[50-52], suggesting the important role of solute in enhancing HPT refining and strengthening by deformation-induced precipitation. Furthermore, the homogeneity in the microhardness values throughout the disks radius (Fig. 8), even after small strain and in the disk centre, thus being independent on the number of turns and strain, suggests that the precipitation of these fine Si precipitates starts immediately after the application of the high initial compressive pressure and strain homogeneously through the whole sample. Therefore, the high compressive stress is responsible for the microstructure formation at the start of deformation through the generation of dislocations interacting among them and with the fine precipitates that arise from the supersaturated solid solution. This gives rise to an ultrafine strain-hardened subgrain structure. This substructure size is, in general, an inverse function of the applied stress, as previous results on ECAP have shown [28,53]. In turn, this ultrafine microstructure is responsible for the high hardness obtained throughout the sample, even at the centre of the disk. After the initial compression, the main effect of the increasing torsional straining is merely to increase gradually the grain boundary misorientation.

It is worth noting that the results shown in the present study indicate that the imposed torsional straining by HPT processing is homogeneous and can be properly evaluated from two-phase systems, being one of these undeformable, such as the Si particles in the Al-7wt%Si alloy, which act as a deformation marker.

5. Conclusions

Disks of as-cast Al-7%Si alloy were processed by HPT under a range of experimental conditions, i.e. different number of turns and two rotation speeds. Optical microscopy and SEM were considered to characterize the aluminium matrix microstructure and the imposed HPT shear strain patterns delineated by the eutectic silicon particles distribution. The main conclusions of this study are as follows:

1. Shear straining by HPT results in monotonic thickness reduction of the primary α cells on the cross-section planes as a function of radius.
2. Shear strain patterns drawn by the non-deforming eutectic silicon particles distribution indicate that the imposed strain is uniform throughout the disk radius and deviation from the ideal torsional shear strain has never been observed.
3. The high initial compressive pressure of 6 GPa prior to torsional straining determines grain refinement in the Al matrix. Additionally, precipitation of

small silicon particles from the supersaturated solid solution is enhanced by this high pressure. These small silicon particles contribute to extra grain refining (~200 nm) and inhibit extended recovery and/or recrystallization during increasing torsional straining.

4. High strengthening is achieved after HPT processing. However, microhardness values are not strain dependent, being similar under different strain paths and throughout the disk diameter. This unusual behaviour observed for this alloy is due to the fact that a very fine initial (sub)grain size is developed during initial compressive straining resulting from the high initial compressive pressure. The subsequent torsional straining just increases monotonically the misorientation of the grain boundaries by transforming LABs into HABs.
5. The improved mechanical strength after HPT processing by grain refining and deformation-induced precipitation, together with eutectic redistribution and homogenization, favouring ductility, opens new possibilities for aluminium casting alloys.

Acknowledgements

Financial support from MICINN (Projects MAT2009-14452 and MAT2012-38962) is gratefully acknowledged.

References

1. R.Z. Valiev, Y. Estrin, Z. Horita, T.G. Langdon, M.J. Zehetbauer, Y.T. Zhu, JOM 58(4) (2006) 33-39.

2. D. Orlov, P. Prasad Bhattacharjee, Y. Todaka, M. Umemoto, N. Tsuji, Scripta Mater. 60 (2009) 893-896.

3. Z. Horita, D.J. Smith, M. Furukawa, M. Nemoto, R.Z. Valiev, T.G. Langdon, J. Mater. Res. 11 (1996) 1880-1890.

4. A.P. Zhilyaev, G.V. Nurislamova, B.-K. Kim, M.D. Baró, J.A. Szpunar, T.G. Langdon, Acta Mater. 51 (2003) 753-765.

5. A.P. Zhilyaev, K. Oh.ishi, T.G. Langdon, T.R. McNelley, Mater. Sci. Eng. A410-411 (2005) 277-280.

6. R.B. Figueiredo, P.R. Cetlin, T.G. Langdon, Mater. Sci. Eng. A 528 (2011) 8198-8204.

7. A.P. Zhilyaev, J.M. García-Infanta, F. Carreño, T.G. Langdon, O.A. Ruano, Scripta Mater. 57 (2007) 763-765.

8. R.B. Figueiredo, M.T.P. Aguilar, P.R. Cetlin, T.G. Langdon, Metall. Mater. Trans. A 42 (2011) 3013-3021.
9. Y. Estrin, A. Molotnikov, C.H.J. Davies, R. Lapovok, J. Mech. Phys. Solids 56 (2008) 1186-1202.
10. H. Jiang, Y.T. Zhu, D.P. Butt, I.V. Alexandrov, T.C. Lowe, Mater. Sci. Eng. A 290 (2000) 128-138.
11. A.P. Zhilyaev, S. Lee, G.V. Nurislamova, R.Z. Valiev, T.G. Langdon, Scripta Mater. 44 (2001) 2753-2758.
12. Z. Yang, U. Welzel, Mater. Lett. 59 (2005) 3406-3409.
13. M. Kai, Z. Horita, T.G. Langdon, Mater. Sci. Eng. A 488 (2008) 117-124.
14. K.V. Rajulapati, R.O. Scattergood, K.L. Murty, Z. Horita, T.G. Langdon, C.C. Koch, Metall. Mater. Trans. A 39 (2008) 2528-2534.
15. J.M. García-Infanta, A.P. Zhilyaev, F. Carreño, O.A. Ruano, J.Q. Su, S.K. Menon, T.R. McNelley, J. Mater. Sci. 45 (2010) 4613-4620.
16. A.P. Zhilyaev, T.G. Langdon, Progr. Mater. Sci. 53 (2008) 893–979.
17. Y. Cao, Y.B. Wang, S.N. Alhajeri, X.Z. Liao, W.L. Zheng, S.P. Ringer, T.G. Langdon, Y.T. Zhu, J. Mater. Sci. 45 (2010) 765-770.
18. Y. Cao, Y.B. Wang, R.B. Figueiredo, L. Chang, X.Z. Liao, M. Kawasaki, W.L. Zheng, S.P. Ringer, T.G. Langdon, Y.T. Zhu, Acta Mater. 59 (2011) 3903-3914.
19. Z. Horita, D.J. Smith, M. Furukawa, M Nemoto M, Valiev RZ, T.G. Langdon, in: T. Chandra, T. Sakai, editors. THERMEC'97. vol. II. Warrendale, PA: The Minerals, Metals and Materials Society; 1997. p. 1937–43.
20. Y.Z. Tian, X.H. An, S.D. Wu, Z.F. Zhang, R.B. Figueiredo, N. Gao, T.G. Langdon, Scripta Mater. 63 (2010) 65-68.
21. J.M. García-Infanta, S. Swaminathan, A.P. Zhilyaev, F. Carreño, O.A. Ruano, T.R. Mcnelley, Mater. Sci. Eng. A 485 (2008) 160-175.
22. J.M. García-Infanta, A.P. Zhilyaev, C.M. Cepeda-Jiménez, O.A. Ruano, F. Carreño, Scripta Mater. 58 (2008) 138-141.
23. S. Swaminathan, J.M. García-Infanta, T.R. McNelley, O.A. Ruano, F.Carreño, J. Mater. Sci. 43 (2008) 7501-7506.
24. A. Vorhauer, R. Pippan, Scripta Mater. 51 (2004) 921-925.
25. J. Cizek, M. Janecek, O. Srba, R. Kuzel, Z. Barnovska, I. Prochazka, S. Dobatkin, Acta Mater. 59 (2011) 2322-2329.
26. Y.Z. Tian, S.D. Wu, Z.F. Zhang, R.B. Figueiredo, N. Gao, T.G. Langdon, Scripta Mater. 65 (2011) 477-480.
27. O.D. Sherby, P.M. Burke, Progr. Mater. Sci., 13 (1968) 323-390.

28. C.M. Cepeda-Jiménez, J.M. García-Infanta, E.F. Rauch, J.J. Blandin, O.A. Ruano, F. Carreño, Metall. Mater. Trans. A 43 (2012) 4224-4236.
29. M. Kawasaki, B. Ahn, T.G. Langdon, Acta Mater. 58 (2010) 919-930.
30. P. Serre, R.B. Figueiredo, N. Gao, T.G. Langdon, Mater. Sci. Eng. A 528 (2011) 3601-3608.
31. G. Sakai, Z. Horita, T.G. Langdon, Mater. Sci. Eng. A 393 (2005) 344-351.
32. Z. Horita, T.G. Langdon, Mater. Sci. Eng. A 410-411 (2005) 422-425.
33. A.P. Zhilyaev, T.R. McNelley, T.G. Langdon, J. Mater. Sci. 42 (2007) 1517-1528.
34. Y. Todaka, M. Umemoto, A. Yamazaki, J. Sasaki, K. Tsuchiya, Mater. Trans. 49 (2008) 7-14.
35. C. Xu, Z. Horita, T.G. Langdon, Acta Mater. 56 (2008) 5168-5176.
36. C. Xu, Z. Horita, T.G. Langdon, J. Mater. Sci. 43 (2008) 7286-7292.
37. L. Balogh, T. Ungár, Y. Zhao, Y.T. Zhu, Z. Horita, C. Xu, T.G. Langdon, Acta Mater. 56 (2008) 809-820.
38. N. Lugo, N. Llorca, J.M. Cabrera, Z. Horita, Mater. Sci. Eng. A 477 (2008) 366-371.
39. A.P. Zhilyaev, A.A. Gimazov, G.I. Raab, T.G. Langdon, Mater. Sci. Eng. A 486 (2008) 123-126.
40. K. Edalati, T. Fujioka, Z. Horita, Mater. Sci. Eng. A 497 (2008) 168-173.
41. K. Edalati, T. Fujioka, Z. Horita, Mater. Trans. 50 (2009) 44-50.
42. K. Edalati, Z. Horita, Mater. Sci. Eng. A 528 (2011) 7514-7523.
43. M. Kawasaki, J. Foissey, T.G. Langdon, Mater. Sci. Eng. A 561 (2013) 118-125.
44. G. Le Roy, J.D. Embury, G. Edward, M.F. Ashby, Acta Metall. 29 (1981) 1509-1522.
45. C.H. Caceres, J.R. Griffiths, Acta Mater. 44 (1996) 25–33.
46. G. Guiglionda, W.J. Poole, Mater. Sci. Eng. A319–321 (2001) 583–587.
47. S.J. Harris, A. O'Neill, J. Boileau, W. Donlon, X. Su, B.S. Majumdar, Acta Mater. 55 (2007) 1681–1693.
48. M.J. Zehetbauer, H.P. Stüwe, A. Vorhauer, E. Schafler, J. Kohout, Adv. Eng. Mater. 5 (2003) 330-337.
49. S. Descartes, C. Desrayaud, E.F. Rauch, Mater. Sci. Eng. A 528 (2011) 3666-3675.
50. J. M. García-Infanta, S. Swaminathan, C.M. Cepeda-Jiménez, T.R. McNelley, O.A. Ruano, F. Carreño, J. Alloy. Compd. 478 (2009) 139-143.
51. C.M. Cepeda-Jiménez, J.M. García-Infanta, A.P. Zhilyaev, O.A. Ruano, F. Carreño, J. Alloy. Compd. 509 (2011) 636-643.
52. C.M. Cepeda-Jiménez, J.M. García-Infanta, A.P. Zhilyaev, O.A. Ruano, F. Carreño, Mater. Sci. Eng. A 528 (2011) 7938-7947.

53. C.M. Cepeda-Jiménez, J.M. García-Infanta, O.A. Ruano, F. Carreño, J. Alloy. Compd. 509 (2011) 8649-8656.

Figure Captions

Figure 1. Schematic illustrations of (a) a quasi-constrained high pressure torsion die, and (b) selected positions for microstructure observation on the cross section of the HPT disks, and for microhardness measurements on the disk surface.

Figure 2. (a) Optical micrograph showing primary Al dendritic cells and eutectic Si particles in the as-cast Al-7wt%Si alloy before processing by HPT. (b) Dendrite size distribution histogram determined by measuring about 1000 dendrites in the as-cast Al-7wt%Si alloy.

Figure 3. Photomontages from optical micrographs showing the microstructure of the disk surface processed by HPT after (a) 0.25, (b) 0.5 and (c) 1 turns. (d) Magnified micrographs of the regions marked in the previous photomontages.

Figure 4. Cross-section optical images of a disk processed by HPT after 0.25 turns: (a) an overview of the whole cross-section; (b) magnified areas taken from the red rectangles in (a) at different radii.

Figure 5. Cross-section images of samples processed by HPT after 0.25, 0.5, 1 and 5 turns. Vertical lines indicate positions where the dendrite thickness was measured, being the red line the centre of the disk.

Figure 6. Average dendrite thickness as a function of the distance from the disk centre after different number of turns at two different rotation speeds: (a) 1 rpm and (b) 0.1 rpm.

Figure 7. Average dendrite thickness as a function of the shear strain for the seven experimental conditions of the HPT processing considered in this investigation.

Figure 8. Vickers microhardness vs. distance through the diameter of the HPT processed samples for different number of turns and two rotation speeds: (a) 1 rpm and (b) 0.1 rpm. The microhardness value for the unprocessed sample is also indicated by a dashed line.

Figure 9. Logarithmic plot of the average dendrite thickness as a function of the shear strain, for the seven experimental conditions of HPT processing considered in this study.

Figure 10. a) Optical micrographs showing the silicon particles, and b) Si particle size distribution histogram determined by measuring about 500 particles in HPT processed Al-7wt%Si alloy by 5 turns and 6 GPa.

Figure 11. Backscattered electrons micrographs at two magnifications of: a) and b) the HPT processed Al-7wt%Si alloy by 0.25 turns, 1rpm and 6 GPa on the center of the disk; and c) and d) after processing by 5 turns, 1rpm and 6 GPa on the periphery of the disk.

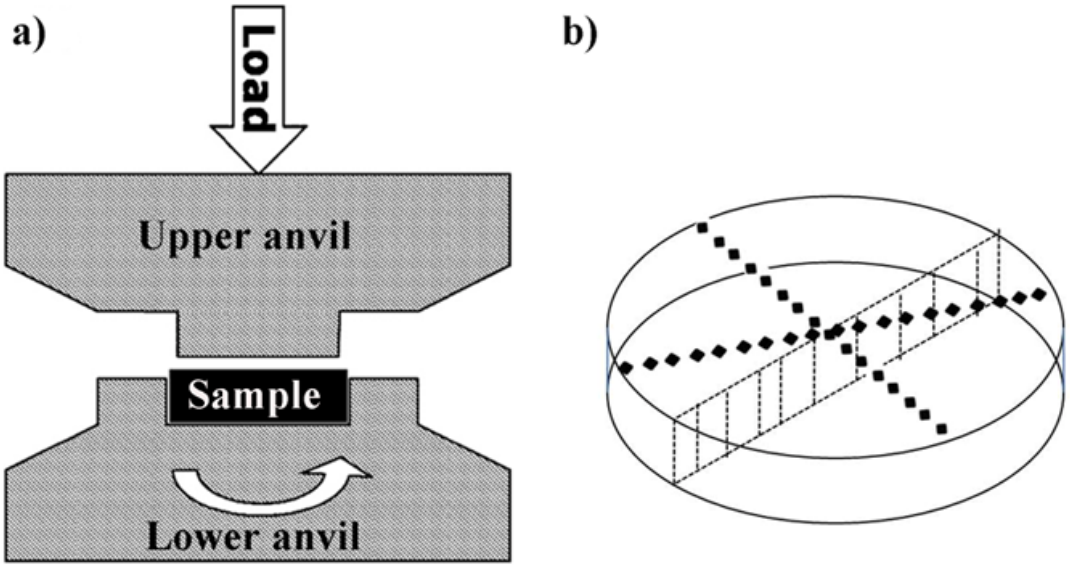

Figure 1. Schematic illustrations of (a) a quasi-constrained high pressure torsion die, and (b) selected positions for microstructure observation on the cross section of the HPT disks, and for microhardness measurements on the disk surface.

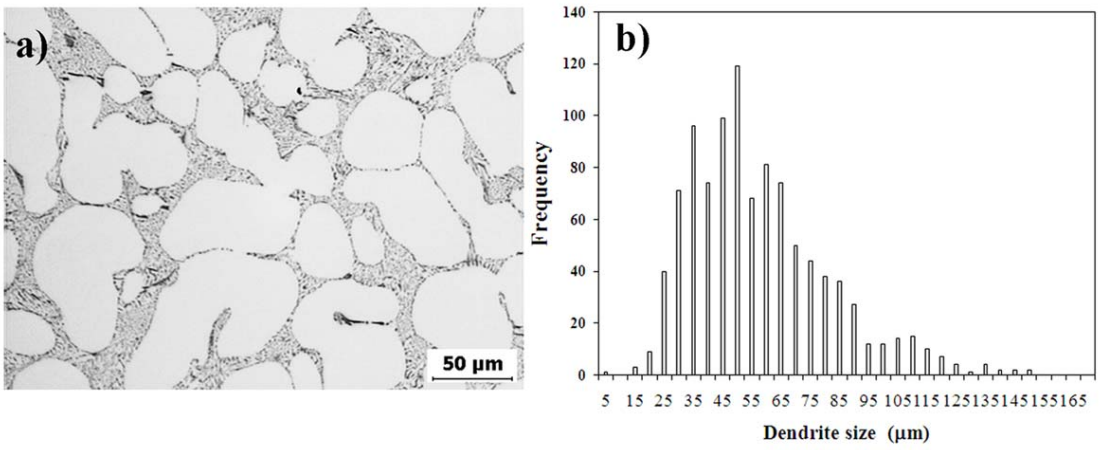

Figure 2. (a) Optical micrograph showing primary Al dendritic cells and eutectic Si particles in the as-cast Al-7wt%Si alloy before processing by HPT. (b) Dendrite size distribution histogram determined by measuring about 1000 dendrites in the as-cast Al-7wt%Si alloy.

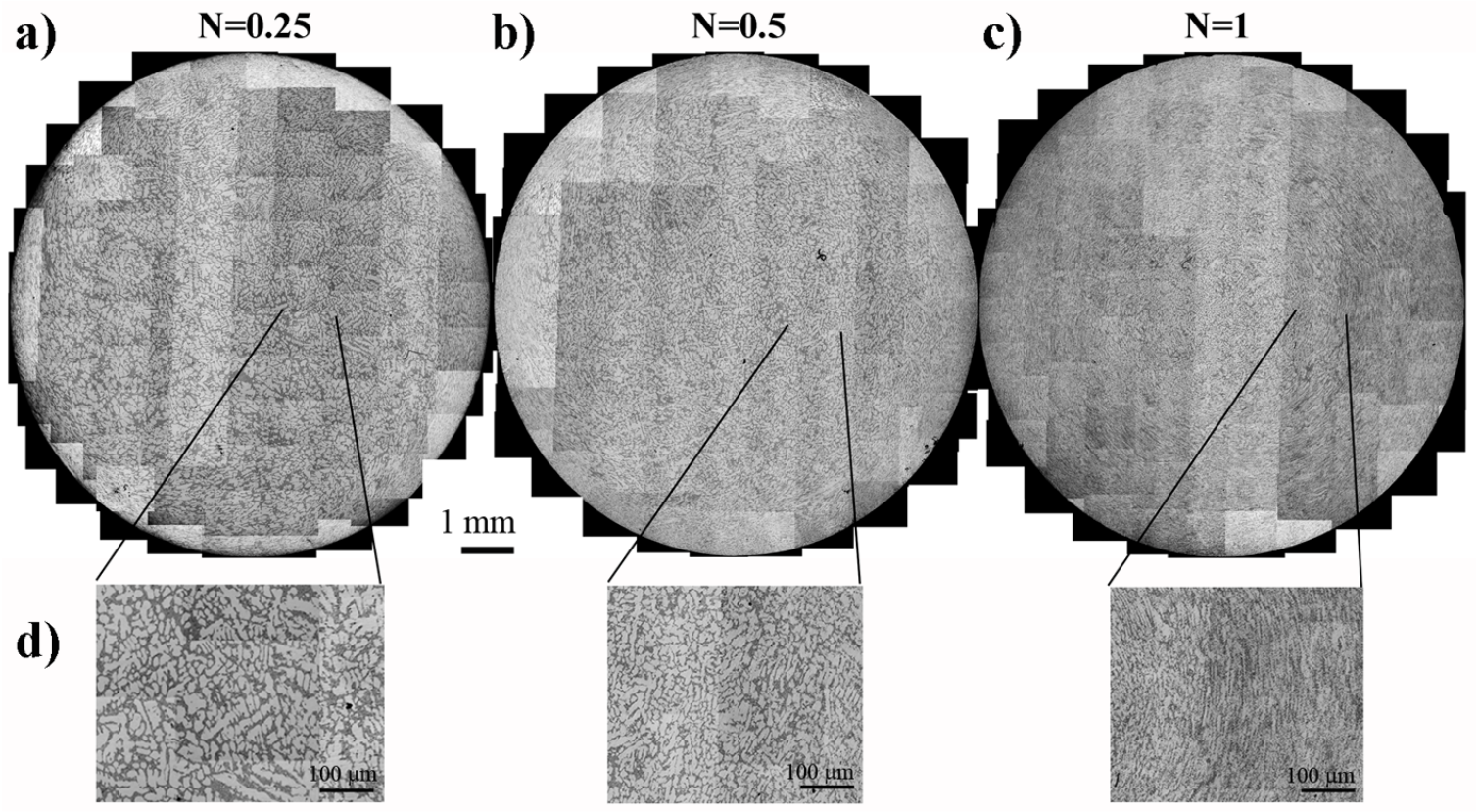

Figure 3. Photomontages from optical micrographs showing the microstructure of the disk surface processed by HPT after (a) 0.25, (b) 0.5 and (c) 1 turns. (d) Magnified micrographs of the regions marked in the previous photomontages.

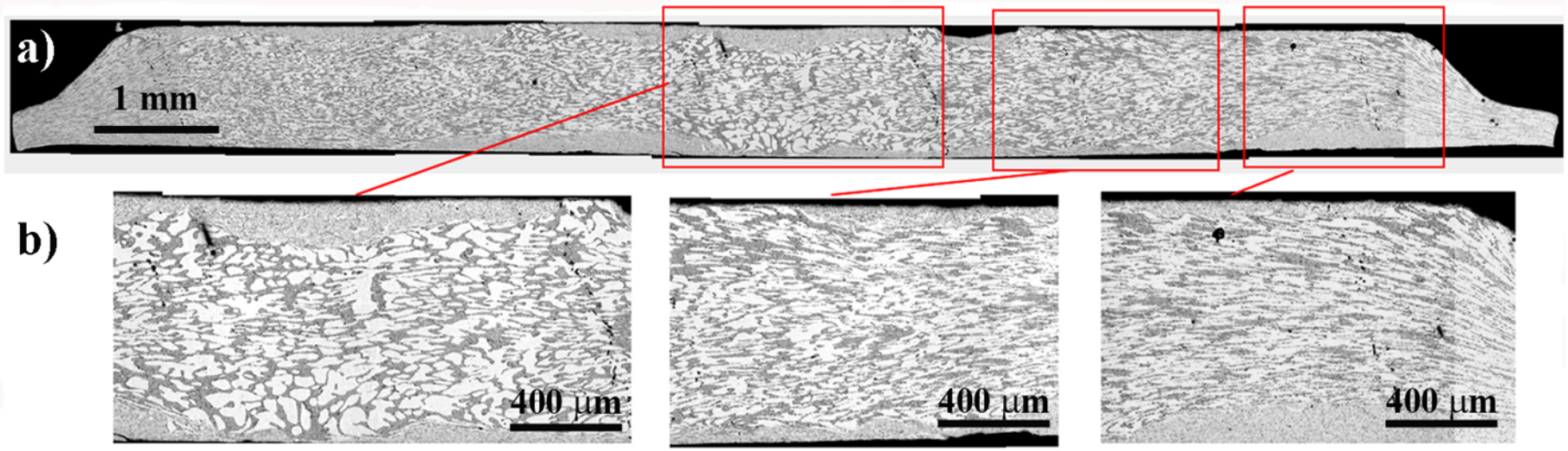

Figure 4. Cross-section optical images of a disk processed by HPT after 0.25 turns: (a) an overview of the whole cross-section; (b) magnified areas taken from the red rectangles in (a) at different radii.

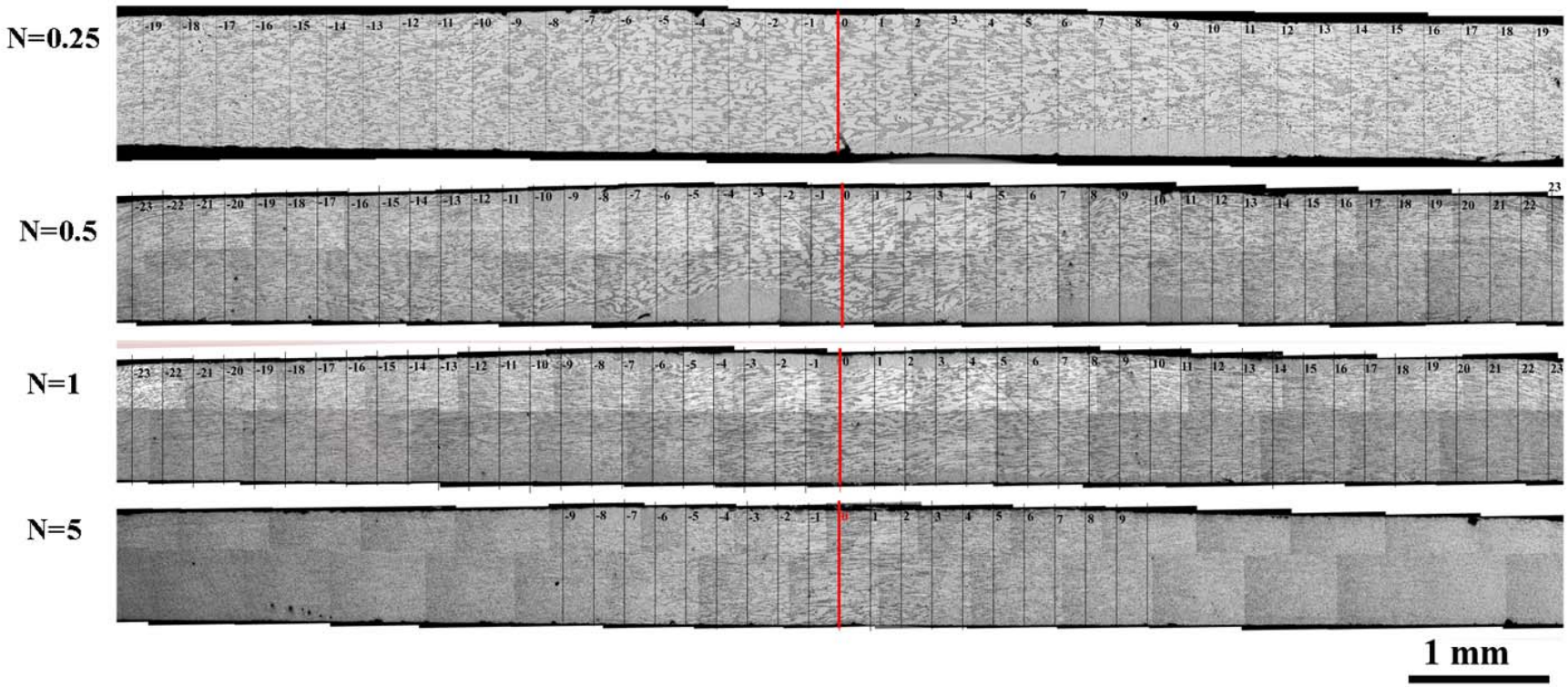

Figure 5. Cross-section images of samples processed by HPT after 0.25, 0.5, 1 and 5 turns. Vertical lines indicate positions where the dendrite thickness was measured, being the red line the centre of the disk.

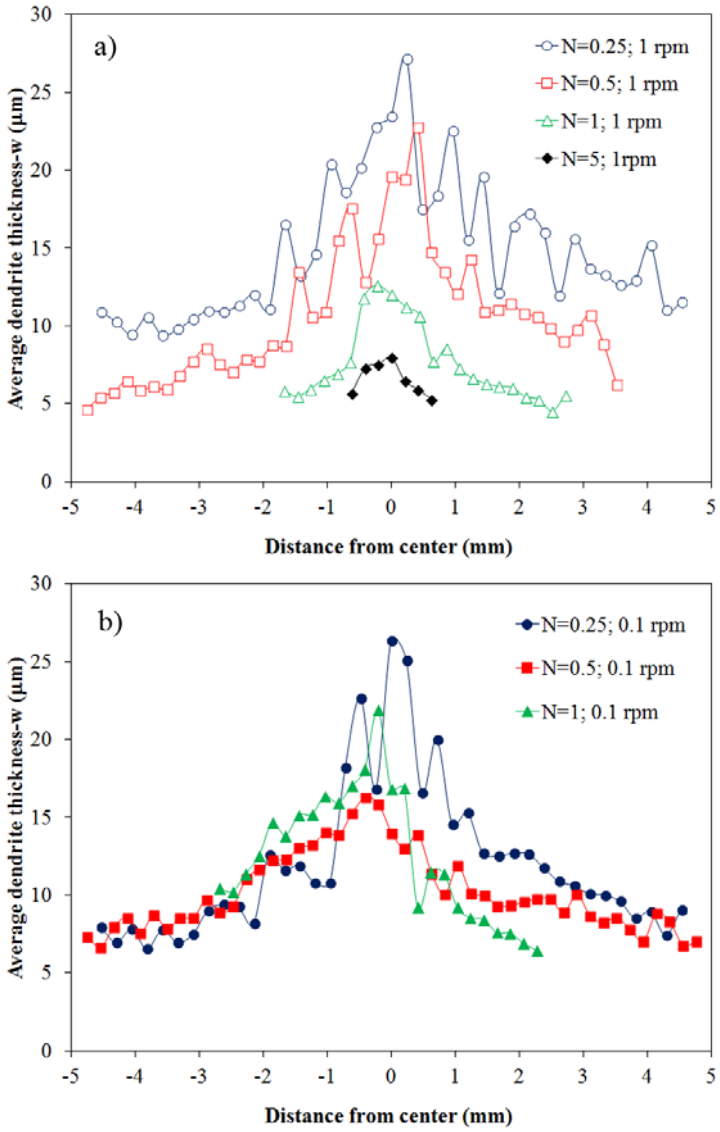

Figure 6. Average dendrite thickness as a function of the distance from the disk centre after different number of turns at two different rotation speeds: (a) 1 rpm and (b) 0.1 rpm.

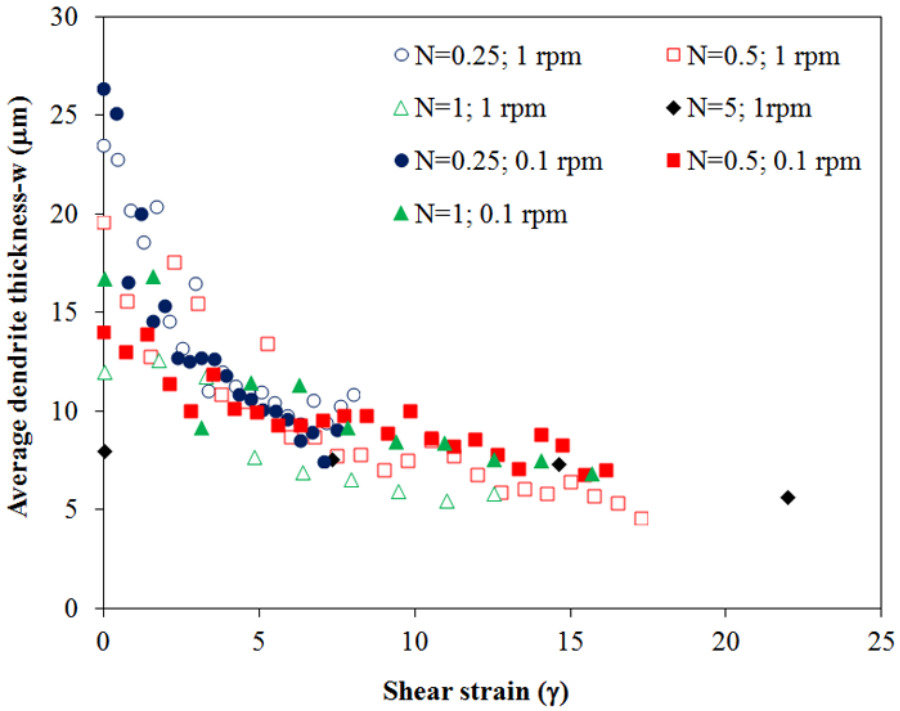

Figure 7. Average dendrite thickness as a function of the shear strain for the seven experimental conditions of the HPT processing considered in this investigation.

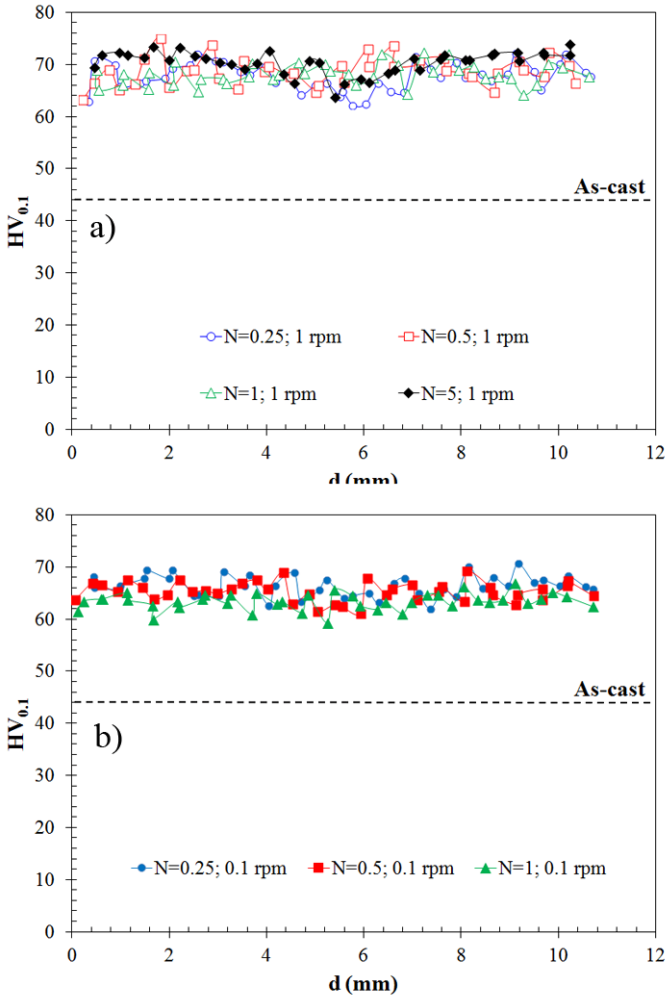

Figure 8. Vickers microhardness vs. distance through the diameter of the HPT processed samples for different number of turns and two rotation speeds: (a) 1 rpm and (b) 0.1 rpm. The microhardness value for the unprocessed sample is also indicated by a dashed line.

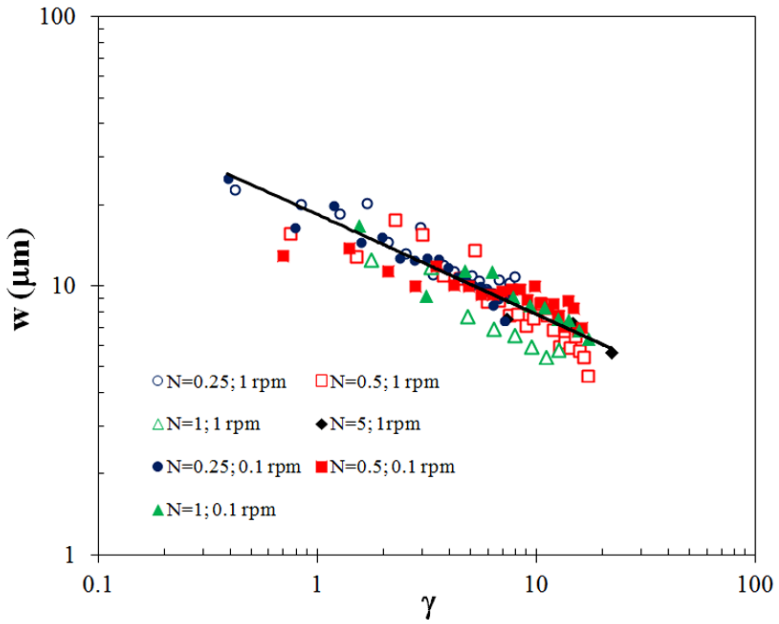

Figure 9. Logarithmic plot of the average dendrite thickness as a function of the shear strain, for the seven experimental conditions of HPT processing considered in this study.

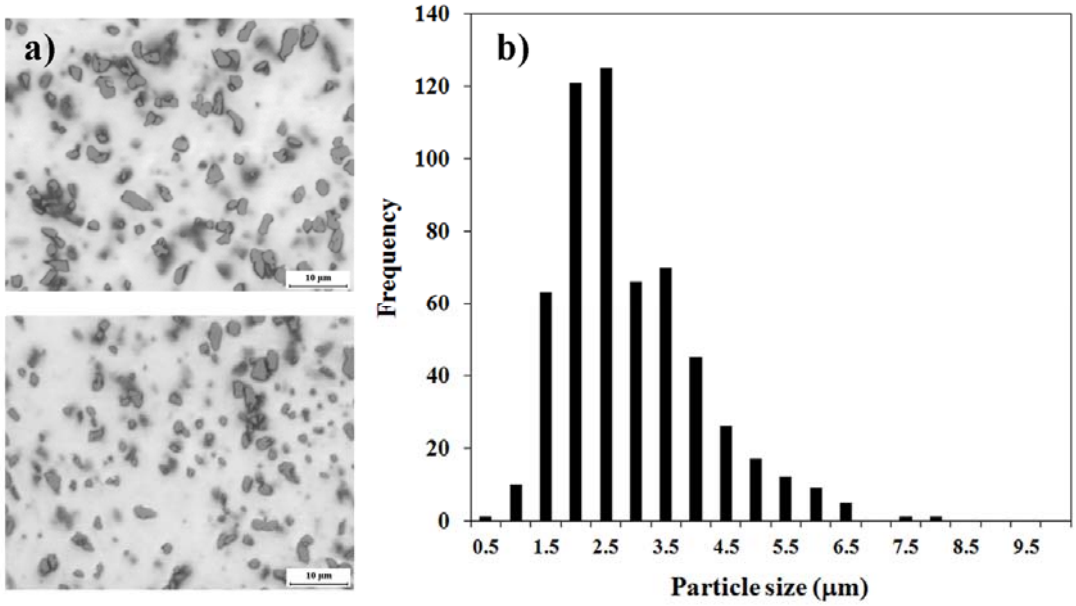

Figure 10. a) Optical micrographs showing the silicon particles, and b) Si particle size distribution histogram determined by measuring about 500 particles in HPT processed Al-7wt%Si alloy by 5 turns and 6 GPa.

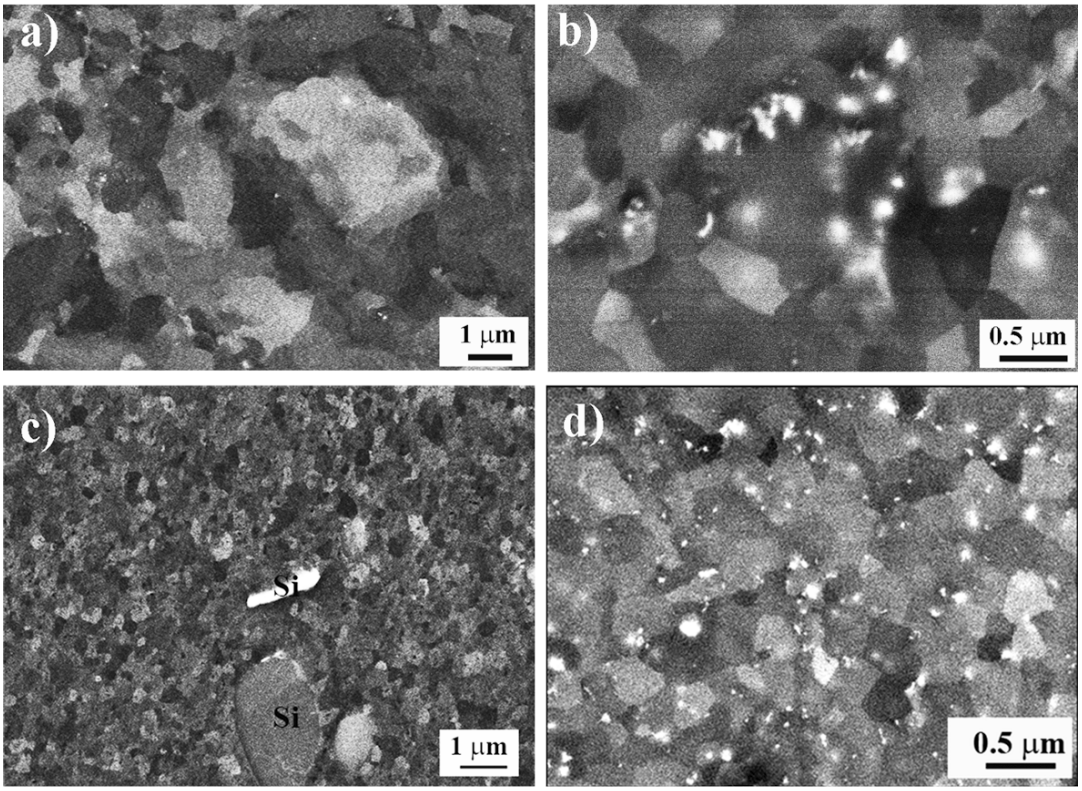

Figure 11. Backscattered electrons micrographs at two magnifications of: a) and b) the HPT processed Al-7wt%Si alloy by 0.25 turns, 1rpm and 6 GPa on the center of the disk; and c) and d) after processing by 5 turns, 1rpm and 6 GPa on the periphery of the disk.